fibers

MDPI

Article

Application of Organosilicon Modifier Based on Tetraethoxysilane for the Production of Heat-Resistant Chrysotile Fibers and Reinforced Cement Composites

Roman Nikolaevich Yastrebinsky *, Vyacheslav Ivanovich Pavlenko, Anna Viktorovna Yastrebinskaya, Andrey Ivanovich Gorodov and Anastasia Vladislavovna Akimenko

Department of Theoretical and Applied Chemistry, Belgorod State Technological University Named after V.G. Shukhov, 308012 Belgorod, Russia; belpavlenko@mail.ru (V.I.P.); karanna1@mail.ru (A.V.Y.); gorodov-andreyy@mail.ru (A.I.G.); nastya-akimenko.2602@yandex.ru (A.V.A.)
* Correspondence: yrndo@mail.ru

Abstract: This research is aimed at obtaining boron-containing nanotubular chrysotile fibers with increased neutron absorption capacity. The possibility of using an organosilicon modifier based on tetraethoxysilane to increase the hydrothermal stability of chrysotile, as well as the strength of nanoreinforced composites based on a cement binder is considered. The mechanisms for the synthesis of heat-resistant nanotubular fibers of the composition $Mg_6(OH)_8SiB_4O_{10}$, which have a chrysotile structure, have been established. To increase the hydrothermal stability of chrysotile, crystalline hydrate phases were localized inside nanotubes using amorphous silica formed as a result of hydrolysis of silicon alkoxide under hydrothermal conditions in an alkaline environment. The modification of chrysotile via amorphous silica increases its hydrothermal stability by 97 °C. It is shown that the introduction of an organosilicon modifier based on tetraethoxysilane into the composition of Portland cement composite material leads to an increase in the structural strength and density of the composite due to the activation of silicate formation processes in the cement matrix, especially under hydrothermal conditions. The experiments showed that the strength of silicon alkoxide-modified samples of composite material increased by 34%.

Keywords: chrysotile asbestos; magnesium hydroborate; modification; tetraethoxysilane; amorphous silica; cement composite; calcium hydrosilicates; microstructure; properties

Citation: Yastrebinsky, R.N.; Pavlenko, V.I.; Yastrebinskaya, A.V.; Gorodov, A.I.; Akimenko, A.V. Application of Organosilicon Modifier Based on Tetraethoxysilane for the Production of Heat-Resistant Chrysotile Fibers and Reinforced Cement Composites. *Fibers* **2023**, *11*, 80. https://doi.org/10.3390/fib11100080

Academic Editors: Francesco Bencardino, Luciano Ombres and Pietro Mazzuca

Received: 11 August 2023
Revised: 11 September 2023
Accepted: 15 September 2023
Published: 22 September 2023

1. Introduction

When developing composites for protection against neutron radiation, special attention is paid to materials with high specific density of hydrogen atoms that effectively slow down fast neutrons [1–4]. Serpentine-containing minerals and metal hydrides, which have increased thermal stability compared to paraffin or polymer neutron moderators are particularly effective [5–12]. In addition, the addition of serpentine fibers can significantly improve the performance of the concrete composite, as well as control cracking [13–15].

The most widely studied and promising filler of composite materials on cement binder is chrysotile asbestos (chrysotile)—a fibrous mineral of the serpentine group, aqueous magnesium silicate $Mg_3Si_2O_5(OH)_4$, the chemical composition of which can vary depending on the deposit. The size difference between tetra- and octahedral layers of chrysotile leads to the formation of nanotubes with an outer diameter of about 25–30 nm [16–18]. Practically, chrysotile is a bundle of interwoven nanotube fibers. The value of chrysotile as a reinforcing component in cement matrix is determined by its high mechanical strength of fibers (tensile strength up to 3000 MPa, modulus of elasticity is $1.6–2.1 \cdot 10^4$ MPa), sorption activity, adhesion to binders, and dispersive filling aggregates, as well as the possibility of forming strong topochemical bonds with them [19]. The distinctive feature of chrysotile asbestos compared to ordinary aggregates is its ability to retain chemically bound water

almost without losses at prolonged exposure to high temperatures up to 450 °C. At higher temperatures, dehydration of chrysotile occurs, including the removal of hydrated water via the cavities of the nanotubes [18].

The possible modification of the surface or internal structure of chrysotile-based nanotube fillers provides a significant increase in the functional characteristics of the developed radiation shielding materials [20,21]. The modification of chrysotile by introducing crystalline hydrate and boron-containing compounds will make it possible to increase the protective properties of the composite material in relation to thermal and superthermal neutrons. The possibility of using boron for the absorption of thermal neutrons and its ability to replace silicon in minerals are already known [22–24]. In this case, the coordination sphere of boron atoms can include hydroxyl groups (unlike silicon) [25,26]. The association of isolated tetrahedrons of $B(OH)_4$ into polyions and the ability of polyions to polymerize at decreasing temperatures leads to the formation of framework boron-containing crystalline hydrate structures [27,28]. It is reasonable to use concrete reinforced with such materials in radiation shielding structures operating at temperatures up to +(300–350) °C without fear of reduction in its protective properties [29].

In the case of radiation and thermal exposure, special active and plasticizing additives that contribute to the strengthening of composite material can play a significant role. For example, the use of amorphous silica as an active additive makes it possible to ensure the process of self-healing of emerging microcracks in concrete and increase the mechanical strength of the structure [30]. Therefore, the use of alkoxysilanes (tetraalkoxysilanes) as an additive in concrete is a promising research field. These substances have the ability to form amorphous silica both at the stage of concrete mixture hardening (due to hydrolysis processes) and at the stage of radiation and thermal heating of the protective composite [31–34]. In addition, it is expected that the use of tetraalkoxysilanes will accelerate the processes of hydrate formation (at early stages) and silicate formation (at later stages) during the cement matrix hardening. This in turn will lead to the densification of concrete structures and increase their strength and density [20,21,35,36].

In this regard, in this work, processes for producing boron-containing nanotubular chrysotile fibers were studied to increase the ability of this material to absorb thermal neutrons. The possibility of using the organosilicon modifier tetraethoxysilane to increase the hydrothermal stability of chrysotile, as well as the strength of nanoreinforced composites based on a cement binder is considered.

2. Materials and Methods

Boron-containing chrysotile was obtained on the basis of a mixture of magnesium oxide, and silicic and boric acids based on the molecular ratio of oxides $MgO:SiO_2:B_2O_3$ = 1.5:0.1:0.9. The ratio of oxides was determined taking into account the condition $MgO:(SiO_2 + B_2O_3)$ = 1.5, which corresponds to the ratio of oxides in natural serpentine. The obtained homogenized mixture was autoclaved in 0.2% NaOH solution at a temperature of 573 K and a pressure of $2.5 \cdot 10^7$ Pa with isothermal exposure for 5 h. At the same time, decreasing the pressure to 10^7 Pa did not affect the formation of a stable serpentine phase. The reaction rate also decreased markedly with the decreasing temperature. Reducing the temperature to 473 K increased the holding time to 24 h. However, this resulted in the formation of shorter boron-containing chrysotile nanotubes. The reaction rate was limited by the composition of the initial mixture: the more silica in the initial mixture, the longer the process of serpentine formation takes place. The alkaline medium promoted the formation of long-fiber cylindrical fibrils.

To study the hydrothermal synthesis of chrysotile, a GSA-0.3 high-pressure reactor was used, designed to carry out chemical reactions under supercritical conditions of high pressure and temperature. All reactor parts in contact with the working environment are made of high-quality corrosion-resistant steel KhN65MV (Hastelloy C-276). The installation is mounted on a frame with a pneumatic lift (Figure 1a). The reactor container consists of an all-metal vessel, which is sealed on top with a flat clamping lid, and a union nut

with additional fastening with six bolts (Figure 1b). The design ensures the tightness of the detachable connection, operational safety, simplicity, and convenience of assembling and disassembling the reactor. The working volume of the vessel is 300 mL, the working pressure is 70 MPa, the maximum operating temperature is 350 °C, the stirrer rotation speed is 50–500 rpm, and the installation power is 2–3 kW. The installed PID controller ensures fairly high stability of temperature control; deviations from the set value do not exceed 2 °C. The pressure gauge has an accuracy class of 1.5.

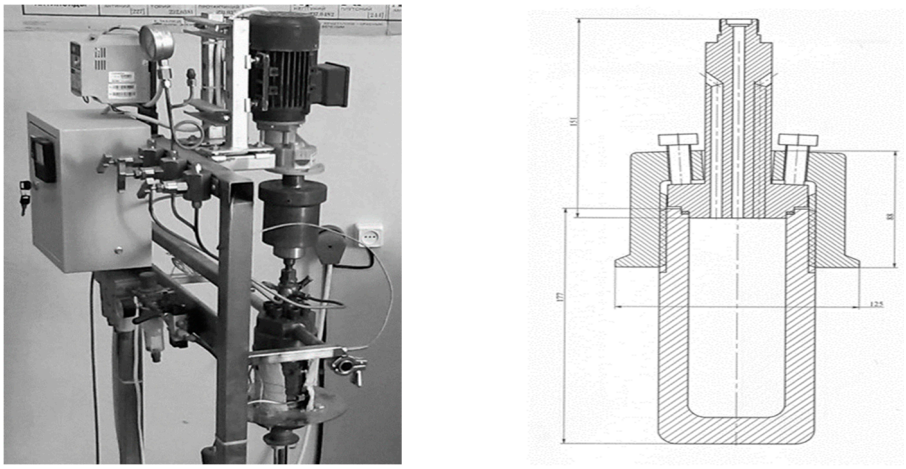

(**a**) (**b**)

Figure 1. Installation (**a**) and sketch of the tank (**b**) of the GSA-0.3 high-pressure reactor.

Comparative studies were carried out using natural chrysotile from the Bazhenov deposit in Russia with the following chemical composition (Table 1).

Table 1. Chemical composition of chrysotile from Bazhenov deposit.

Content (wt. %)						
SiO_2	MgO	Al_2O_3	Fe_2O_3	FeO	H_2O_{cryst}	H_2O_{ads}
42.1	41.99	0.53	1.3	0.24	12.99	1.42

The Bazhenov chrysotile deposit is the largest in the world and is located on the eastern slope of the Ural ridge. It is distinguished by a wide range of chrysotile fibers in length and strength.

Pure tetraethoxysilane (TEOS) was used as an organosilicon modifier for analysis with a mass fraction of the basic substance not less than 98.5% (TU 2637-187-44493179-2014, Russia).

Portland cement of CEM 0 52.5H grade (GOST 31108-2020, Russia) with the content of Portland cement clinker not less than 95% was used as a binder to obtain the composite material. The chemical composition of Portland cement is presented in Table 2.

Table 2. Chemical composition of Portland cement CEM 0 52.5H.

Content (wt. %)					
CaO	SiO_2	Al_2O_3	Fe_2O_3	MgO	SO_3
65.8	20.8	4.9	3.5	2.9	2.1

Magnetite iron ore concentrate from the Lebedinsky deposit of Kursk Magnetic Anomaly (KMA) (TU14-9288-84, Russia) with a main phase magnetite content of 66.76 wt. % was used as a dispersed aggregate of composites. The chemical composition of magnetite concentrate is presented in Table 3.

Table 3. Chemical composition of magnetite concentrate [wt. %].

Content (wt. %)							
Fe_{gen}	Fe_3O_4	FeO	SiO_2	Al_2O_3	CaO	MgO	$K_2O + Na_2O$
68.82	66.76	27.61	4.25	0.18	0.14	0.34	0.14

A Superplasticizer C-3 (TU 5745-001-97474489-2007, Russia) was used to increase the water-reducing ability of the cement–magnetite mixture.

The composite was prepared by sequentially mixing magnetite, chrysotile, and Portland cement, followed by the addition of a solution containing water, superplasticizer C-3, and tetraethoxysilane (TEOS). The composite mixture was placed in collapsible molds, followed by vibration compaction and hardening for three days. The frequency of vertical vibrations of a vibrating platform with a mold filled with a composite mixture is (2900 ± 100) min^{-1}, the amplitude of vertical vibrations is 0.5 ± 0.05 mm, and the amplitude of horizontal vibrations is no more than 0.1 mm.

Next, the composite was removed from the mold for hardening under standard conditions for 28 days or hydrothermal treatment in a steaming chamber according to the 3-8-4 regime (temperature set—holding—temperature decreased, hour). The error in maintaining the set temperature in the steaming chamber is no more than 2 °C in the range from 20 °C to 100 °C.

The composition of the composite mixture is presented in Table 4.

Table 4. Composition of the raw material mixture of nano-reinforced cement composite.

Content (wt. %)						
Magnetite	Chrysotile	CEM 0 52.5H	Superplasticizer	TEOS	Water	Σ
70.00	7.45	16.50	0.10	1.00	4.95	100

Compressive strength was determined on composite samples measuring 100 × 100 × 100 mm on a press based on the results of at least 5 direct measurements. The sample was loaded under an axial load until failure with a constant rate of load increase (0.6 ± 0.2) MPa/s.

X-ray phase analysis and X-ray diffraction analysis were performed on an X-ray diffractometer "Dron-2.0" with Cu_{cc}—radiation (λ_{cc} = 1.542 Å) and nickel filter using the ASTM Card Index. The spectra were recorded with an MSTR-4 ionization counter at Breg angles from 4 to 80°. The X-ray diffraction patterns were interpreted according to the ASTM Card Index using the program "Crystallographica SearchMath" according to the intensity of the maximum peak, angle 2θ, and interplanar distance d. Powder samples of the material with a dispersion of no more than 10 microns were used for analysis.

The microstructure of the materials was investigated via scanning electron microscopy (SEM) in secondary (SE) electron mode using a high-resolution TESCAN MIRA 3LMU scanning electron microscope (TESCAN ORSAY HOLDING, Brno, Czech Republic). When preparing samples, a conductive chromium coating several nm thick was applied to freshly chipped composite samples using magnetron sputtering using a Quorum Q150T S Plus setup.

Quantitative chemical and elemental analysis of the solid phases of materials was carried out via electron probe microanalysis using an X-MAX 50 energy dispersive spectrometer (Oxford Instruments NanoAnalysis, High Wycombe, Great Britain).

Transmission electron microscopy (TEM) was performed using a JEM-2100 electron microscope (JEOL, Tokyo, Japan).

Differential thermal (DTA), thermogravimetric (TG), and differential thermogravimetric (DTG) analyses of the samples were performed using an STA-449 F1 Iupiter derivatograph (Germany) at a heating rate of 10 deg/min in the air in an alundum crucible. Powder samples of the material with a dispersion of no more than 10 microns were used for analysis.

3. Results and Discussion

X-ray phase analysis of synthesized boron-containing chrysotile using CuK_{α}-radiation (Ni filter) showed the formation of two main phases: hydrosilicate phase of chrysotile of composition $Mg_3Si_2O_5(OH)_4$ (with interplanar distance d = 7.3600; 4.5650; 3.6600; 2.5470; 2.4510 Å); and crystalline hydrate phase of magnesium hydroborate of composition $MgB_3O_3(OH)_5 \cdot 5H_2O$ (with interplanar distance d = 3.9080; 3.3570; 3.0248; 2.6046; 2.5051 Å), as well as the presence of amorphous halo in the interplanar interval d = 7–4 Å (Figure 2, Table 5). The numbers of diffraction characteristics in Table 4 correspond to the numbers of phases in the X-ray diffraction patterns of Figure 2.

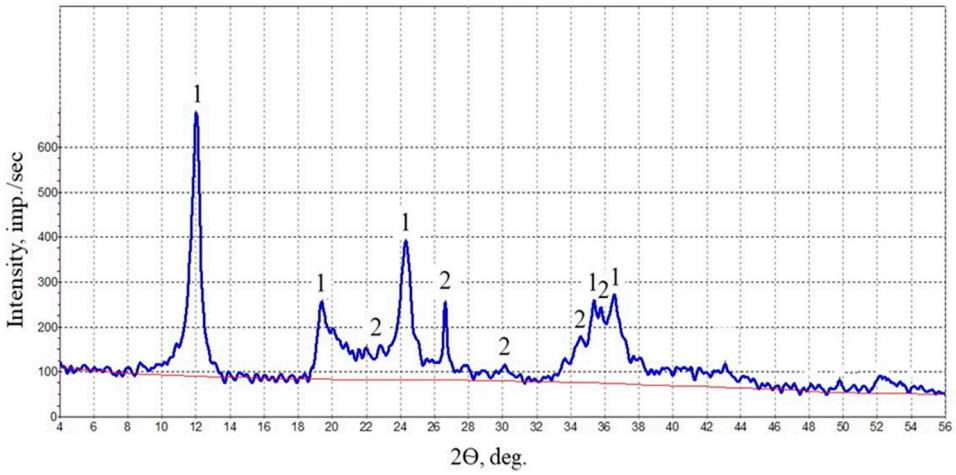

Figure 2. X-ray diffraction patterns of synthesized boron-containing chrysotile: 1—$Mg_3Si_2O_5(OH)_4$; 2—$MgB_3O_3(OH)_5 \cdot 5H_2O$.

Table 5. Diffraction characterization of synthesized boron-containing chrysotile.

№	Angle 2θ, °	Square	Int. [imp/sec]	Half-Width	d [Å]	% max.
1	12.000	932.727	1475	0.6325	7.3600	100.00
1	19.350	555.789	427	1.3026	4.5650	28.95
1	24.350	617.193	803	0.7689	3.6600	54.44
1	35.350	406.247	467	0.8705	2.5470	31.66
1	36.550	525.467	515	1.0210	2.4510	34.92
2	22.800	146.483	213	0.6866	3.9080	14.44
2	26.600	106.066	461	0.2299	3.3570	31.25
2	28.900	51.367	61	0.8375	3.0248	4.14
2	34.600	256.668	285	0.8995	2.6046	19.32
2	35.800	351.695	456	0.7713	2.5051	30.92

Therefore, boron completely replaces silicon in the crystal lattice of chrysotile with the formation of hydroborate. The formed magnesium hydroborate contains up to 62.5 wt. % of chemically bound water, including 30.4 wt. % of the water of constitution and 32.1 wt. % of the water of crystallization.

Electron-probe microanalysis of the synthesized compound showed the formation of boron-containing chrysotile of composition $Mg_6(OH)_8SiB_4O_{10}$ with the content of boron atoms 8.59 wt.% (taking into account the hydrogen content) (Figure 3).

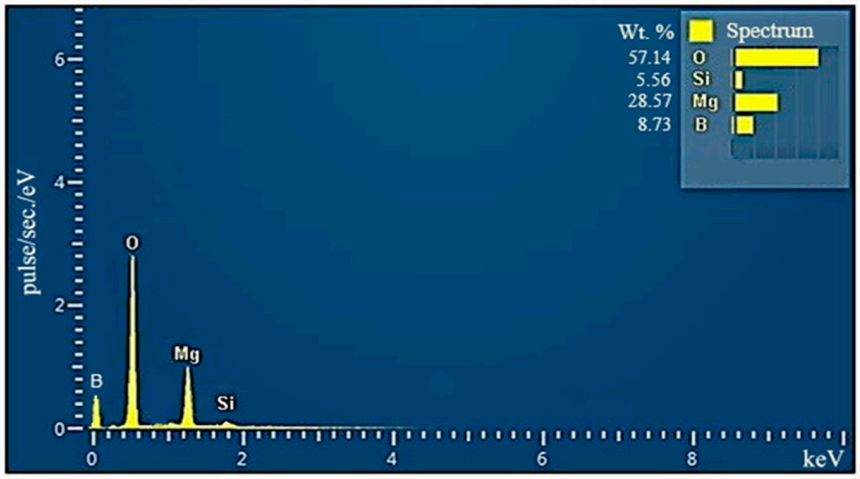

Figure 3. X-ray spectrum of boron-containing chrysotile.

The study of the microstructure of synthesized chrysotile using scanning electron spectroscopy (SEM) indicates the formation of nanotubular fibers with lengths ranging from a few microns to several millimeters with an outer diameter of about $2.5 \cdot 10^{-8}$ m (Figure 4). Increasing the synthesis time up to 10 h promoted the growth of nanotubes and the degree of their homogeneity along their length.

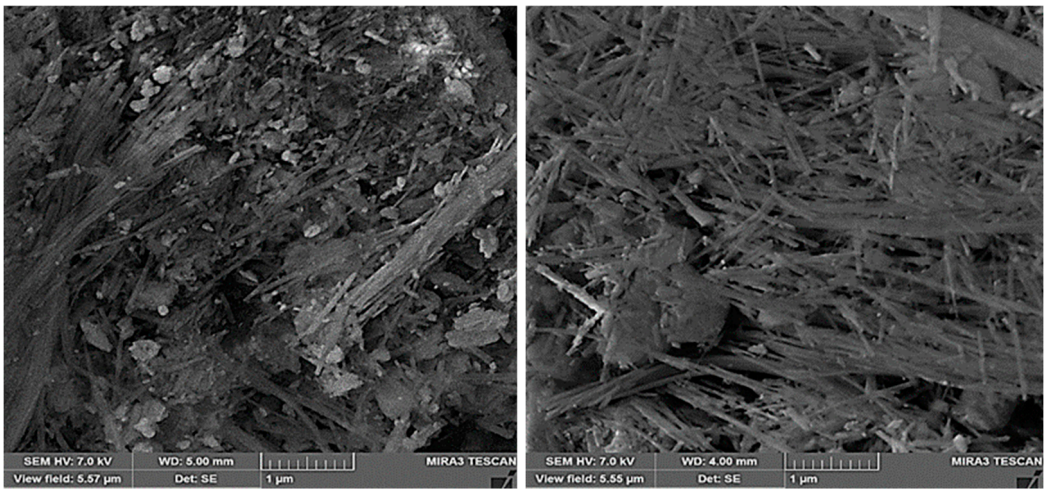

(**a**) (**b**)

Figure 4. Microstructure of synthesized boron-containing chrysotile (573 K; $2.5 \cdot 10^8$ Pa) with isothermal exposure: (**a**) 5 h; (**b**) 10 h.

As a result of the studies conducted using transmission electron microscopy (TEM), it was found that the inner diameter of nanotubes of synthesized boron-containing chrysotile is ~8 nm (80 Å) with an outer diameter of ~25 nm (250 Å) (Figure 5). At the same time, the inner diameter of nanotubes of natural chrysotile can reach up to 10–15 nm (100–150 Å) [37–39].

In this connection, it seems possible to increase the hydrothermal stability of natural or synthesized chrysotile by filling nanotubular cavities with hydrated amorphous silica, in the structure of which silicon atoms retain one hydroxyl group each. In the works of Ailer and Dolimora, it was also demonstrated [40] that such polymeric structures can be obtained via the polymerization of methacrylonitric acid in water under standard conditions in acidic or alkaline media. Under these conditions, silica polymerizes into spherical particles with diameters less than 20 Å, which bind into a three-dimensional gel mass, retaining sorbed water molecules [40]. Thermal treatment of such a system hydrolyzed in the presence of

chrysotile will produce amorphous silica, which will plug the nanotubes, preventing the processes of high-temperature dehydration.

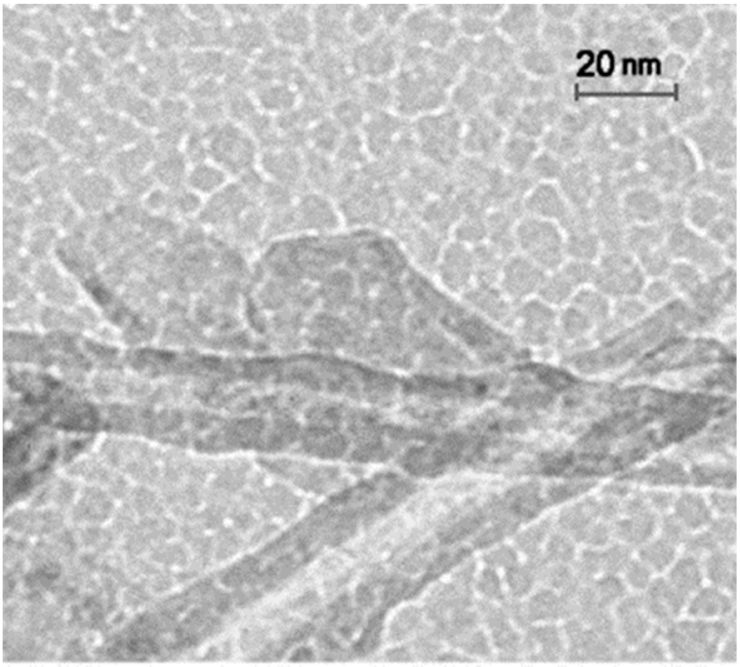

Figure 5. Synthesized boron-containing chrysotile (TEM).

To confirm this assumption, we modified boron-containing chrysotile with tetraethoxysilane (TES) in ethanol solution followed by hydrolysis of silicon alkoxide under hydrothermal conditions in an alkaline medium (pH = 10) for 6 h. According to [41], when water content exceeds the stoichiometric ratio, polysilicic acids are formed by the reaction as follows:

$$Si(OC_2H_5)_4 + 4H_2O \rightarrow H_4SiO_4 + 4C_2H_5OH \quad (1)$$

The formed polysilicic acid at the initial stages of polymerization has a particle size of not more than 10–20 Å, which allows it to fill the edge cavities of nanotubes. The use of an alkaline medium makes it possible to preserve the nanotubular structure of chrysotile.

Similar studies were carried out on natural chrysotile from the Bazhenov deposit. In this case, before the modification of natural chrysotile, it was treated with an aqueous solution of acetic acid (pH = 4.5). This enabled the freeing of the cavities of nanotubes from impurities. To eliminate the acid residues, a thorough rinsing of natural chrysotile with water was performed. However, it is important to note that the use of other acids led to the disruption of the structure of chrysotile [42].

According to the results of differential thermal analysis (DTA) [29,42] of TEOS hydrolyzed in an alkaline medium, the transition of gel cluster to amorphous cluster was found at 260 °C. This result is in agreement with previous studies showing the formation of amorphous silica from organosilicon oligomers [31]. Therefore, the modified chrysotile was heat treated at this temperature to form amorphous silica in the nanotube cavities. The formation of amorphous silica is possible not only inside the nanotubes but also on their surface due to the pre-adsorption of colloidal particles due to van der Waals forces (Figure 6). This type of interaction is possible due to differently charged surfaces of chrysotile and colloidal silica, carrying, respectively, positive and negative charges.

Figures 7 and 8 show derivatograms of unmodified and amorphous silica-modified boron-containing chrysotile.

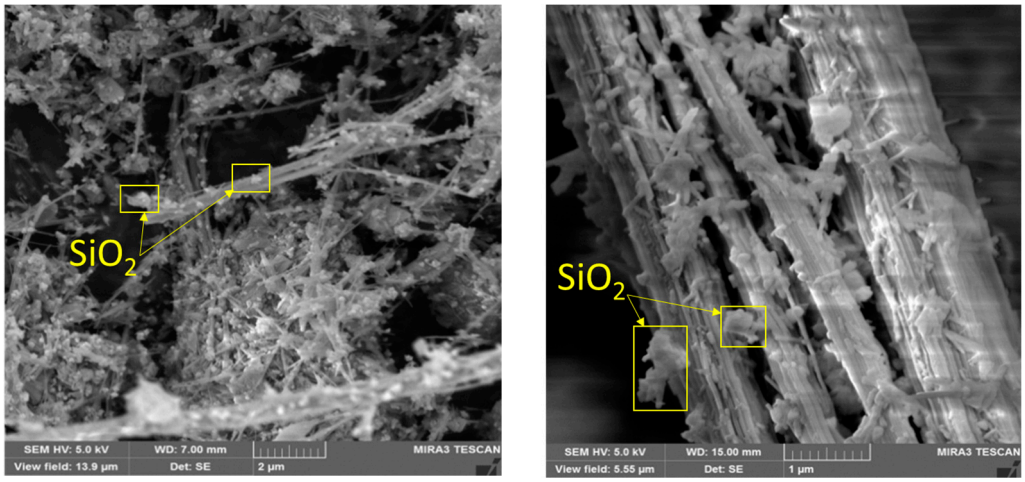

(**a**) (**b**)

Figure 6. Microstructure of synthesized boron-containing (**a**) and natural (**b**) chrysotile modified with amorphous silica.

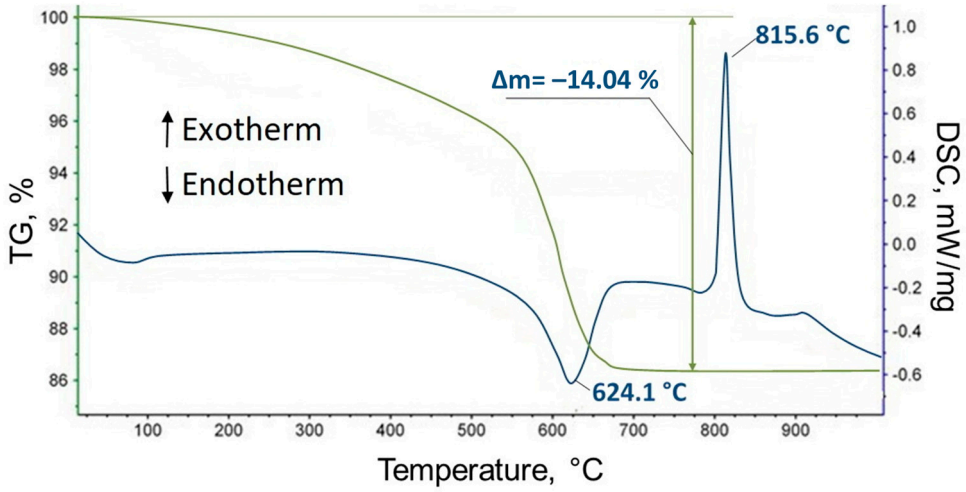

Figure 7. Derivatogram of synthesized boron-containing chrysotile.

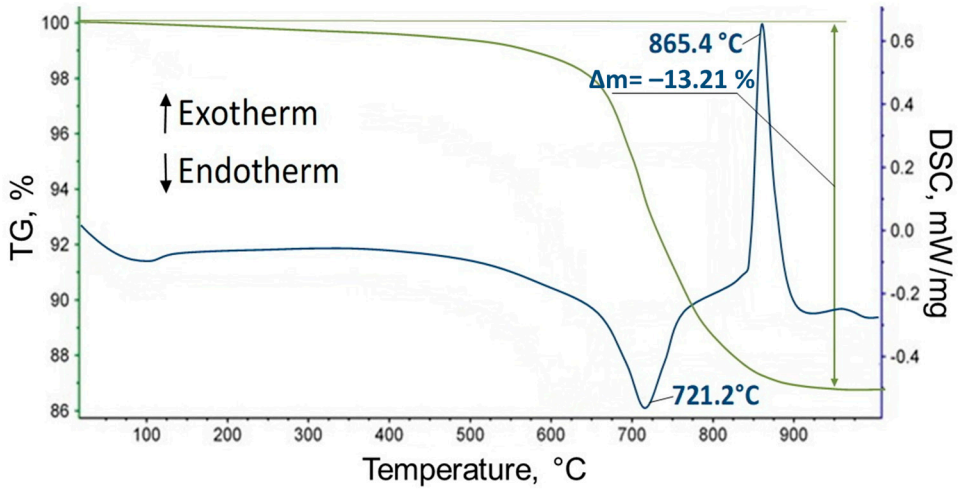

Figure 8. Derivatogram of boron-containing chrysotile modified with amorphous silica.

Two endothermic effects of different intensities were recorded on the thermograms of the studied samples. One effect corresponds to the removal of adsorption water at 100 °C,

and the other to the removal of water of constitution (chemically bound in the form of OH-groups) at 624.1 °C and 721.2 °C, respectively, for unmodified and modified chrysotile. However, an interesting phenomenon was observed in the case of modified chrysotile: the endoeffect associated with the removal of water of constitution was shifted to the high-temperature region by almost 100 °C. This indicates increased hydrothermal stability of the modified material. It is also worth noting that the modified chrysotile showed a broadening of the endoeffect and a gentler course of the mass loss curve in the high-temperature region. This indicates dehydration processes that continue even at temperatures up to 900 °C.

The intensive exothermic effect in the interval between 815 °C and 865 °C indicates the ordering of the structure of forsterite $Mg_2[SiO_4]$, formed during the dehydration of chrysotile [43]. The absence of thermal effects in the region of 400–500 °C indicates the perfection of the crystal lattice of synthesized boron-containing chrysotile.

In the framework of the research, we studied the effect of TEOS additive on the strength characteristics of nano-reinforced composites based on Portland cement binder. The research was carried out using magnetite concentrate and modified boron-containing chrysotile as fillers.

It was found that at early stages of hardening of cement mixture under standard conditions the strength increase is practically not observed (Table 6). At the same time, the introduction of TEOS above 1 wt.% slightly reduces the strength of the composite due to the ongoing processes of hydrolysis and a decrease in the rate of cement hydration.

Table 6. Study of compressive strength of composite samples with different TEOS content (curing under standard conditions).

Age of Samples (Days)	Compressive Strength without Additive (MPa)	Compressive Strength with TEOS Additive (wt. %) (MPa)			
		0.5%	1.0%	1.5%	2.0%
1	10.1 ± 1.6	10.1 ± 1.6	10.2 ± 1.6	10.2 ± 1.6	8.3 ± 1.6
3	25.3 ± 1.6	24.4 ± 1.6	26.3 ± 1.6	24.3 ± 1.6	22.1 ± 1.6
7	34.2 ± 1.8	35.8 ± 1.8	36.2 ± 1.8	32.2 ± 1.8	30.3 ± 1.8
14	42.1 ± 1.8	42.2 ± 1.8	44.3 ± 1.8	40.2 ± 1.8	38.3 ± 1.8
28	45.2 ± 1.8	46.4 ± 1.8	48.2 ± 1.8	44.3 ± 1.8	41.8 ± 1.8
28 *	40.4 ± 1.8	44.2 ± 1.8	46.4 ± 1.8	43.4 ± 1.8	40.2 ± 1.8

*—drying to constant weight at 300 °C.

Starting from 7 days of hardening, a gradual increase in the strength of the material is observed. Probably, it is explained by the formation of colloidal silica and its interaction with lime formed during cement hydration. However, when TEOS is added above 1.5 wt. %, a decrease in the strength of the composite is observed due to the ongoing processes of TEOS hydrolysis and the formation of colloidal silica. This requires an additional amount of water molecules, which in turn slows down the process of cement hydration. The conducted experiments showed a significant increase in strength (up to 15%) in concrete samples that contained TEOS additive in the amount of 1 wt. % after 28 days of hardening and were subjected to heat treatment at 300 °C (Table 6).

A similar situation is observed when studying the strength of composites subjected to hydrothermal treatment in the steaming chamber according to the mode 3-8-4 (temperature rise—exposure—temperature drop, hour). Thus, on the samples of composites containing 1 wt. % TEOS additive and dried to constant weight at 110 °C, the increase in compressive strength amounted to 19% in comparison with the samples without additive (Table 7).

Table 7. Strength of composite samples subjected to hydrothermal treatment with different TEOS content.

Treatment Temperature (°C)	Compressive Strength (MPa) Depending on TEOS Content (wt. %)				
	0%	**0.5%**	**1.0%**	**1.5%**	**2.0%**
Drying at 110 °C	47.2 ± 1.8	50.3 ± 1.8	56.1 ± 1.8	54.2 ± 1.8	51.8 ± 1.8
Drying at 300 °C	40.4 ± 1.8	45.5 ± 1.8	54.2 ± 1.8	50.3 ± 1.8	47.3 ± 1.8

In this study, it was found that the heat treatment of composite samples at 300 °C increases the strength gain by 34% compared to samples without TEOS additive. These results are reflected in Figure 9, which shows the dependence of compressive strength gain of composite samples depending on the TEOS content in them.

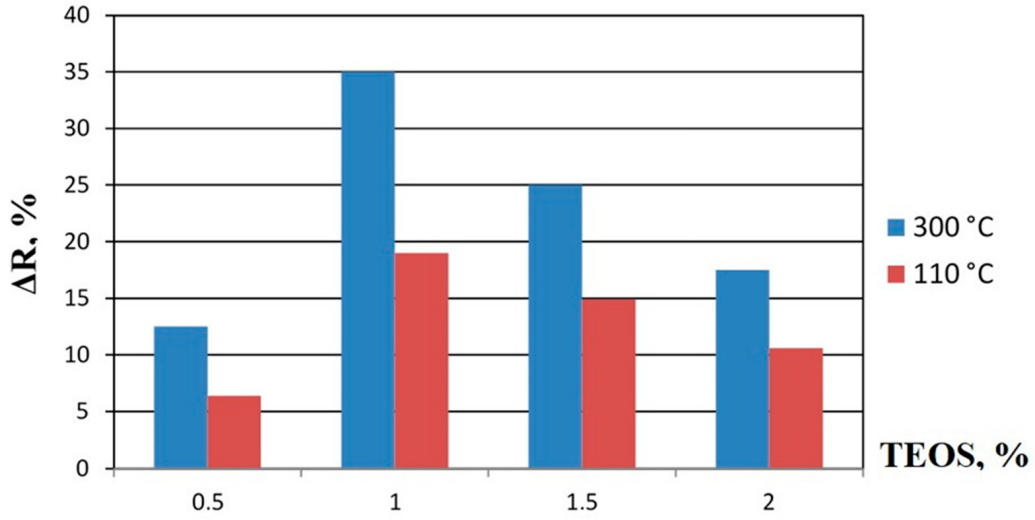

Figure 9. Dependence of the compressive strength gain (ΔR) of heat-treated composite samples on the TEOS content in them.

This may be caused by the formation of amorphous silica in the composite structure during heat treatment, which increases the rate of cement hydration and leads to the formation of ordered structures of calcium hydrosilicates:

$$4SiO_2 + 5Ca(OH)_2 + H_2O \rightarrow Ca_3Si_3O_8(OH)_2 + Ca_2SiO_4 \cdot 5H_2O \quad (2)$$

Additional hydrosilicates structure the cement matrix, giving it increased strength and density. These processes are consistent with the data on the use of nanodispersed silica additives in cement-sand concrete [44,45].

According to the results of the studies, it was found that the formation of amorphous silica in the composite volume originates from colloidal silica at a temperature of 260 °C. This process is carried out as a result of hydrolysis of TEOS in the alkaline environment of cement mixture according to the scheme

$$Si(OC_2H_5)_4 + 4H_2O \rightarrow H_4SiO_4 + 4C_2H_5OH \overset{110^{\circ}C}{\rightarrow} SiO_2 \cdot 2H_2O \overset{260^{\circ}C}{\rightarrow} SiO_2 + 2H_2O \quad (3)$$

As a result of the microstructure analysis of composite samples obtained under hydrothermal conditions and heat treated at 300 °C, it was found that the structure of composites without TEOS additive is characterized by a significant amount of needle-shaped calcium hydroaluminates ($Ca_4Al_6O_{13} \cdot 3H_2O$) on the surface of aggregate (magnetite and chrysotile). These hydroaluminates are the result of the initial hydration stage of clinker minerals (Figure 10a). The addition of silicon alkoxide (TEOS) and the processes of amorphization of colloidal silica accelerate the hydration of clinker minerals and form a finely

porous pile of calcium hydrosilicates ($Ca_3Si_3O_8(OH)_2$), which leads to the formation of a more homogeneous matrix, increased strength and density of the composite (Figure 10b).

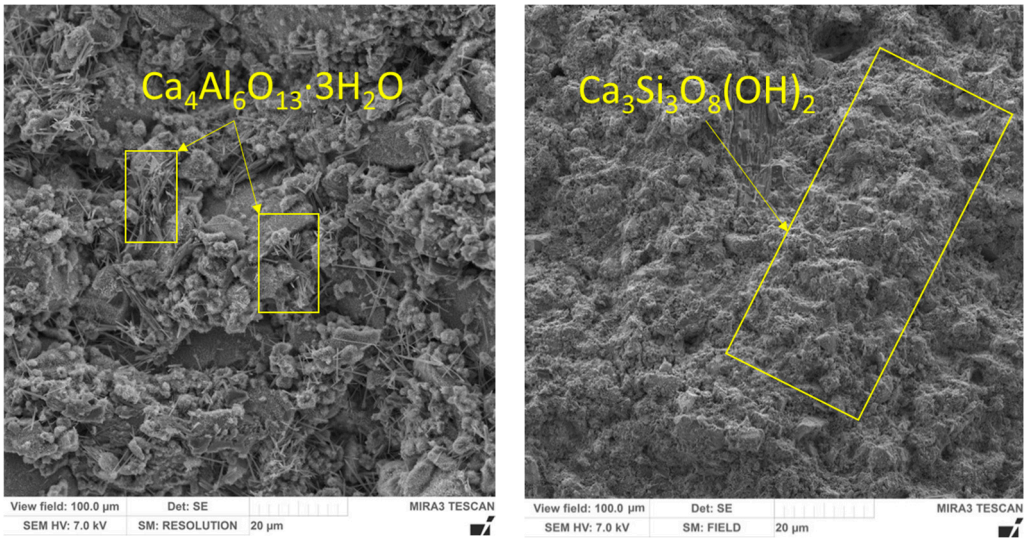

(**a**) (**b**)

Figure 10. Microstructure of composite without TEOS additive (**a**) and with TEOS additive (**b**) after hydrothermal treatment and drying at 300 °C.

The assumptions made are confirmed by the data of X-ray phase analysis of the hydrated cement–lime mixture based on Portland cement of CEM 0 52.5H grade with (Figure 11) and without (Figure 12) TEOS addition, subjected to thermal-moisture (hydrothermal) treatment with subsequent drying at 300 °C. The diffraction characteristics of the main phases are presented in Tables 8 and 9.

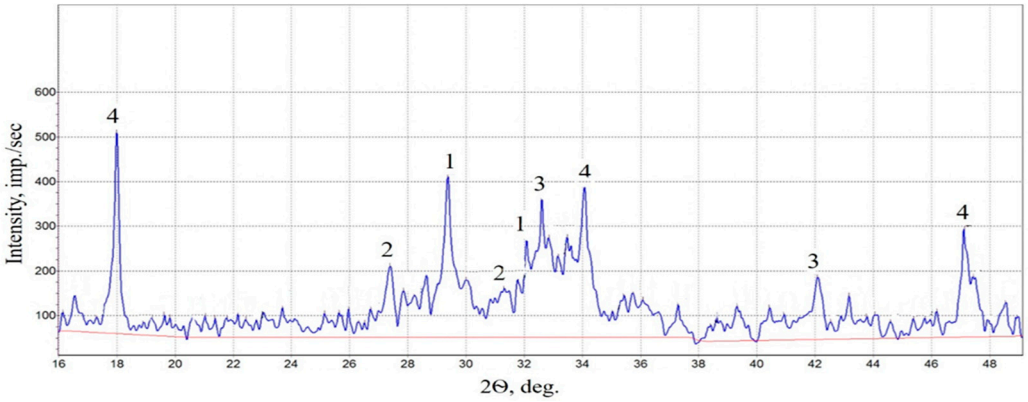

Figure 11. X-ray diffraction pattern of hydrated cement mixture after hydrothermal treatment and drying at 300 °C: 1—β-$Ca_2SiO_4 \cdot 0.5H_2O$; 2—$Ca_4Al_6O_{13} \cdot 3H_2O$; 3—$Ca_5(OH)_2Si_6O_{16} \cdot 4H_2O$; 4—$Ca(OH)_2$.

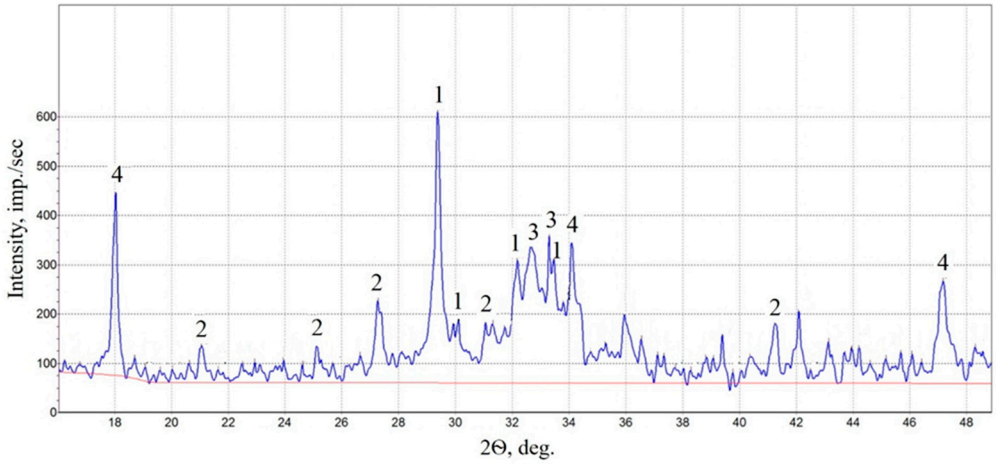

Figure 12. X-ray diffraction pattern of hydrated cement mixture with TEOS additive after hydrothermal treatment and drying at 300 °C: 1—$Ca_3Si_3O_8(OH)_2$; 2—$Ca_2SiO_4 \cdot H_2O$; 3—Ca_2SiO_4; 4—$Ca(OH)_2$.

Table 8. Diffraction characterization of the main phases of the cement–lime mixture after drying at 300 °C.

№	Angle 2θ. °	Square	Int. [imp/sec]	Half-Width	d (Å)	% max.
1	29.380	123.538	363	0.3403	3.0399	80.49
1	32.100	64.629	221	0.2924	2.7883	49.00
2	27.400	57.451	161	0.3568	3.2549	35.70
2	31.500	69.030	117	0.5900	2.8400	25.94
3	32.600	156.441	316	0.4951	2.7466	70.07
3	42.100	51.907	136	0.3817	2.1462	30.16
4	18.000	87.424	451	0.1938	4.9279	100.00
4	34.080	134.121	336	0.3992	2.6307	74.50
4	47.100	78.586	238	0.3302	1.9294	52.77

Table 9. Diffraction characterization of the main phases of cement mixture with TEOS additive after drying at 300 °C.

№	Angle 2θ. °	Square	Int. [imp/sec]	Half-Width	d (Å)	% max.
1	29.380	127.599	555	0.2299	3.0399	100.00
1	29.920	38.149	126	0.3028	2.9863	22.70
1	32.180	110.159	248	0.4442	2.7815	44.68
2	20.620	10.560	40	0.2640	4.3073	7.21
2	24.620	3.325	41	0.0811	3.6158	7.39
2	27.260	51.335	167	0.3074	3.2713	30.09
2	41.260	35.609	121	0.2943	2.1880	21.80
3	32.660	176.383	281	0.6277	2.7417	50.63
3	33.300	61.177	312	0.1961	2.6905	56.22
4	18.020	73.242	379	0.1933	4.9225	68.29
4	34.080	146.192	291	0.5024	2.6307	52.43
4	47.160	80.213	207	0.3875	1.9271	37.30

The analysis of X-ray diffraction patterns of additive-free samples shows, along with calcium hydrosilicates β-$Ca_2SiO_4 \cdot 0.5H_2O$ and $Ca_5(OH)_2Si_6O_{16} \cdot 4H_2O$ (with interplanar distance d = 3.0399; 2.7883; 2.7466; 2.1462 Å), the presence of calcium hydroaluminate phases $Ca_4Al_6O_{13} \cdot 3H_2O$ (with interplanar distance d = 3.2549; 2.8400 Å) [46]. The presence of hydroaluminates characterizes a looser structure of the cement stone, and consequently a decrease in the strength of the composite. In the X-ray diffraction patterns of samples of Portland cement stone with TEOS additive, which was obtained under similar conditions, the presence of hydroaluminates is practically not observed—the cement framework is mainly represented by calcium hydrosilicate phases $Ca_3Si_3O_8(OH)_2$, $Ca_2SiO_4 \cdot H_2O$ (with interplanar distance d = 3.0399; 2.9863; 2.7815; 4.3073; 3.6158; 3.2713; 2.1880 Å), and hydrated lime in the form of portlandite $Ca(OH)_2$ (with interplanar distance d = 4.9225; 2.6307; 1.9271 Å). At the same time, the TEOS additive slightly reduces the intensity of portlandite lines due to the binding of lime by amorphous silica and the formation of calcium silicates Ca_2SiO_4. The formation of additional silicate structure is reflected in the strength increase in composite material (Table 7).

The effect of increasing strength is comparable to adding microsilica to a concrete mixture, for example, in the works of Lukpanov, Faghihmaleki, and Nazari [47,48]. However, the proposed method is more technologically advanced since it uses the addition of a modifier to the mixing water and its uniform distribution in the concrete mixture. In addition, this method is more economical since it requires only a 1.0 wt. % modifier.

Thus, the studied composite material containing modified chrysotile asbestos, upon prolonged heating, retains chemically bound water, and, consequently, hydrogen atoms, which characterizes its high protective properties against fast neutrons. In addition, the content of boron atoms in chrysotile increases the protective properties of the material from thermal neutrons. Cement chrysotile composite can be effectively used as a radiation protection material for nuclear power plants at operating temperatures up to 300 °C.

4. Conclusions

The mechanisms for the synthesis of heat-resistant nanotubular chrysotile fibers of the composition $Mg_6(OH)_8SiB_4O_{10}$ due to the introduction of boron-containing compounds into their structure have been determined; these fibers exhibited increased hydrothermal stability due to the localization of crystalline hydrate phases and the filling of the edge cavities of the nanotubes with hydrated amorphous silica. The modification of the inner cavity of chrysotile nanotubes with amorphous silica increases its hydrothermal stability by 97 °C. Increasing the hydrothermal stability of chrysotile leads to the retention of hydrated water in it, and, consequently, hydrogen atoms, at higher temperatures. This is important for maintaining the high neutron-protective properties of the cement chrysotile composite during radiation-thermal heating of the material.

It is shown that the introduction of an organosilicon modifier based on tetraethoxysilane into the composition of composite material leads to an increase in the structural strength and density of the composite due to the intensification of silicate formation processes in the cement matrix, especially in hydrothermal conditions. This is due to the formation of amorphous silica in the composite structure during heat treatment, which increases the rate of cement hydration and leads to the formation of ordered structures of calcium hydrosilicates. The strength gain on the samples of composite material modified with silicon alkoxide amounted to 34%.

5. Direction for Future Research

Future research will be aimed at studying the radiation-protective characteristics of the developed material and assessing its radiation resistance under long-term exposure to neutron and gamma radiation. In addition, there are plans to measure the volumetric stability (strength) of the resulting concrete composite at relatively high temperatures.

Author Contributions: Formal analysis, V.I.P.; Conceptualization, R.N.Y. and V.I.P.; Methodology, R.N.Y.; Investigation, R.N.Y., A.V.Y. and A.V.A.; Data curation, A.I.G. and A.V.A.; Writing—original draft preparation, A.V.Y.; Writing—review and editing, R.N.Y.; Funding acquisition, V.I.P. All authors have read and agreed to the published version of the manuscript.

Funding: This work was realized using the equipment of the High Technology Center at BSTU named after V.G. Shukhov, the framework of the State Assignment of the Ministry of Education and Science of the Russian Federation, project No. FZWN-2023-0004.

Institutional Review Board Statement: Not applicable.

Informed Consent Statement: Not applicable.

Data Availability Statement: Not applicable.

Conflicts of Interest: The authors declare no conflict of interest.

References

1. Lomonosov, A.A.; Lyapin, A.I. Low-power reactors. Development prospects in Russia and abroad. *Trends Dev. Sci. Educ.* **2023**, *98*, 204–207. [CrossRef]
2. Pronskikh, V. Problems of nuclear technologies and radiation safety. *Digit. Sch. Philos. Lab* **2020**, *3*, 6–24. [CrossRef]
3. Yastrebinsky, R.N.; Pavlenko, V.I.; Karnauhov, A.A.; Cherkashina, N.I.; Yastrebinskaya, A.V. Thermal stability of titanium hydride modified by the electrochemical deposition of titanium metal. *Mater. Res. Express* **2020**, *7*, 106519. [CrossRef]
4. Jóźwiak-Niedźwiedzka, D.; Lessing, P.A. 9—High-density and radiation shielding concrete. In *Developments in the Formulation and Reinforcement of Concrete*, 2nd ed.; Mindess, S., Ed.; University of British Columbia: Vancouver, BC, Canada, 2019; Volume 3, pp. 193–228. [CrossRef]
5. Muta, H.; Tanaka, T.; Ohishi, Y.; Kurosaki, K.; Hishinuma, Y.; Yamanaka, S.; Muroga, T. Properties of Cold-Pressed Metal Hydride Materials for Neutron Shielding in a D–T Fusion Reactor. *Plasma Fusion Res.* **2015**, *10*, 3405021. [CrossRef]
6. Vynogradov, D.V.; Voevodin, V.M.; Tykhonovskyi, M.A.; Kolodii, I.V. Influence of the structural state of zirconium on the sorption–desorption parameters of hydrogen. *Mater. Sci. Vol.* **2013**, *49*, 70–76. [CrossRef]
7. Yastrebinsky, R.; Pavlenko, V.; Karnauhov, A.; Cherkashina, N.; Yastrebinskaya, A.; Gorodov, A. Radiation Resistance of a Structural Material Based on Modified Titanium Hydride. *Sci. Technol. Nucl. Install.* **2021**, *2021*, 6658431. [CrossRef]
8. Neklyudov, I.M.; Borodin, O.V.; Bryk, V.V.; Voyevodin, V.N. Problem of Radiation Resistance of Structural Materials of Nuclear Power. In *Progress in High Energy Physics and Nuclear Safety. NATO Science for Peace and Security, Series B: Physics and Biophysics*; Begun, V., Jenkovszky, L.L., Polański, A., Eds.; Springer: Dordrecht, The Netherlands, 2009; Volume 1, pp. 259–277. [CrossRef]
9. Abo-El-Enein, S.A.; El-Hosiny, F.I.; El-Gamal, S.M.A.; Amin, M.S.; Ramadan, M. Gamma radiation shielding, fire resistance and physicochemical characteristics of Portland cement pastes modified with synthesized Fe_2O_3 and ZnO nanoparticles. *Constr. Build. Mater.* **2018**, *173*, 687–706. [CrossRef]
10. Anopko, D.V.; Honchar, O.A.; Kochevykh, M.O.; Kushnierova, L.O. Radiation protective properties of fine-grained concretes and their radiation resistance. *IOP Conf. Ser. Mater. Sci. Eng.* **2020**, *907*, 012031. [CrossRef]
11. Abulfaraj, W.H.; Salah, M.K. Evaluation of ilmenite serpentine concrete and ordinary concrete as nuclear reactor shielding. *Radiat. Phys. Chem.* **1994**, *44*, 139–148. [CrossRef]
12. Larionov, V.V.; Varlachev, V.A.; Xu, S. Accumulation of hydrogen in titanium exposed to neutron irradiation. *Int. J. Hydrogen Energy* **2020**, *45*, 15294–15301. [CrossRef]
13. Tayeh, B.A.; Akeed, M.H.; Qaidi, S.; Bakar, B.H.A. Influence of microsilica and polypropylene fibers on the fresh and mechanical properties of ultra-high performance geopolymer concrete (UHP-GPC). *Case Stud. Constr. Mater.* **2022**, *17*, e01367. [CrossRef]
14. Aisheh, Y.I.A.; Atrushi, D.S.; Akeed, M.H.; Qaidi, S.; Tayeh, B.A. Influence of polypropylene and steel fibers on the mechanical properties of ultra-high-performance fiber-reinforced geopolymer concrete. *Case Stud. Constr. Mater.* **2022**, *17*, e01234. [CrossRef]
15. Başaran, B.; Kalkan, İ.; Beycioğlu, A.; Kasprzyk, I. A Review on the Physical Parameters Affecting the Bond Behavior of FRP Bars Embedded in Concrete. *Polymers* **2022**, *14*, 1796. [CrossRef] [PubMed]
16. Kumzerov, Y.A.; Parfeneva, L.S.; Smirnov, I.A.; Krivchikov, A.I.; Zvyagina, G.A.; Fil, V.D.; Misiorek, H. Thermal and acoustic properties of chrysotile asbestos. *Phys. Solid State* **2005**, *47*, 357–360. [CrossRef]
17. Cheng, L.K.; Bosenberg, W.R.; Tang, C.L. Growth and characterization of low temperature phase barium metaborate crystals. *J. Cryst. Growth (North-Holl.)* **1988**, *89*, 553–559. [CrossRef]
18. Trittschack, R.; Grobéty, B. The dehydroxylation of chrysotile: A combined in situ micro-Raman and micro-FTIR study. *Am. Mineral.* **2013**, *98*, 1133–1145. [CrossRef]
19. Bodalyov, I.; Malkov, A.A.; Korytkova, E.N. Effect of Temperature Treatment on the Interaction of Nanotubular Magnesium Silicate Mg3Si2O5(OH)(4) with Titanium Tetrachloride and Water Vapors. *Russ. J. Appl. Chem.* **2012**, *85*, 1319–1326. [CrossRef]
20. Potapov, V.; Gorev, D. Physical and chemical characteristics of nansilica (sol, nanopowder) and microsilica. *Fundam. Res.* **2018**, *6*, 23–29. [CrossRef]
21. Sanchez, F.; Sobolev, K. Nanotechnology in concrete—A review. *Constr. Build. Mater.* **2010**, *24*, 2060–2071. [CrossRef]

22. Yastrebinskii, R.N. Attenuation of Neutron and Gamma Radiation by a Composite Material Based on Modified Titanium Hydride with a Varied Boron Content. *Russ. Phys. J.* **2018**, *60*, 2164–2168. [CrossRef]
23. Yastrebinskii, R.N.; Bondarenko, G.G.; Pavlenko, V.I. Attenuation of Photon and Neutron Radiation Using Iron–Magnetite–Serpentinite Radiation-Protective CompositeInorganic Materials. *Appl. Res.* **2017**, *8*, 275–278. [CrossRef]
24. Bubnova, R.S.; Filatov, S.K. High-Temperature borate crystal chemistry. *Z. Für Krist.-Cryst. Mater.* **2013**, *228*, 395–428. [CrossRef]
25. Belokoneva, E.L. Borate crystal chemistry in terms of the extended OD theory: Topology and symmetry analysis. *Crystallogr. Rev.* **2005**, *11*, 151–198. [CrossRef]
26. Antsygin, V.D.; Dashevsky, O.Y.; Solntsev, V.P.; Mashkovtsev, R.I.; Tsvetkov, E.G. Origin of defects in nonlinear BBO crystals. *Proc. SPIE* **2002**, *4751*, 247–251. [CrossRef]
27. Nagaytsev, Y.V. The mobilization of ore elements in the course of metamorphic reactions and processes. *Int. Geol. Rev.* **1988**, *30*, 1084–1091. [CrossRef]
28. Pelissari, P.I.B.G.B.; Pandolfelli, V.C.; Carnelli, D.; Bouville, F. Refractory interphase and its role on the mechanical properties of boron containing nacre-like ceramic. *J. Eur. Ceram. Soc.* **2020**, *40*, 165–172. [CrossRef]
29. Kany, A.M.I.; El-Gohary, M.I.; Kamal, S.M. Thermal, epithermal and thermalized neutron attenuation properties of ilmenite-serpentine heat resistant concrete shield. *Radiat. Phys. Chem.* **1994**, *44*, 157–160. [CrossRef]
30. Perevislov, S. Investigation of the Phase Composition and Analysis of the Properties of Sintered and Hot-Pressed Materials Based on Silicon Nitride. *Refract. Ind. Ceram.* **2022**, *63*, 66–73. [CrossRef]
31. Shilova, O.A. Synthesis and structure features of composite silicate and hybrid TEOS-derived thin films doped by inorganic and organic additives. *J. Sol-Gel Sci. Technol.* **2013**, *68*, 387–410. [CrossRef]
32. Chukalkin, Y.G. Amorphization of oxides under irradiation with fast neutrons. *Phys. Solid State* **2013**, *55*, 1714–1717. [CrossRef]
33. Sickafus, K.E.; Grimes, R.W.; Valdez, J.A. Radiation-induced amorphization resistance and radiation tolerance in structurally related oxides. *Nat. Mater.* **2007**, *6*, 217–223. [CrossRef] [PubMed]
34. Bakaleinikov, L.A.; Zamoryanskaya, M.V.; Kolesnikova, E.V. Silicon dioxide modification by an electron beam. *Phys. Solid State* **2004**, *46*, 1018–1023. [CrossRef]
35. Abdelgadera, H.S.; Fediukb, R.S.; Kurpinskaa, M.; Khatibc, J.; Muralid, G.; Baranovb, A.V.; Timokhinb, R.A. Mechanical properties of two-stage concrete modified by silica fume. *Mag. Civ. Eng.* **2019**, *89*, 26–38. [CrossRef]
36. Yastrebinskii, R.N.; Bondarenko, G.G.; Pavlenko, V.I. Radiation Hardening of Constructional Cement–Magnetite–Serpentinite Composite under Gamma Irradiation at Increased Dos. *Inorg. Mater. Appl. Res.* **2017**, *8*, 691–695. [CrossRef]
37. Roveri, N.; Falini, G.; Foresti, E. Geoinspired synthetic chrysotile nanotubes. *J. Mater. Res.* **2006**, *21*, 2711–2725. [CrossRef]
38. Vakhrushev, S.B.; Ivanov, A.; Kumzerov, Y.A.; Naberezhnov, A.A. Investigation of longitudinal vibrations of OH groups in chrysotile asbestos by neutron scattering and polarized infrared spectroscopy. *Phys. Solid State* **2011**, *53*, 416–420. [CrossRef]
39. Dobrovolskaya, I.P.; Popryadukhin, P.V.; Khomenko, A.Y. Structure and characteristics of chitosan-based fibers containing chrysotile and halloysite. *Polym. Sci. Ser.* **2011**, *53*, 418–423. [CrossRef]
40. Dollimore, D. Silica chemistry. *Nature* **1980**, *283*, 510. [CrossRef]
41. Lin, C.C.; Basil, J.D. 29Si NMR, Sec and Ftir Studies of The Hydrolysis and Condensation of Si(OC2H5)4 and Si2O(OC2H5)6. Materials Research Society symposia proceedings. *Mater. Res. Soc.* **2011**, *73*, 585–590. [CrossRef]
42. Pavlenko, V.I.; Yastrebinsky, R.N.; Sokolenko, I.V. Nanotube chrysotile fillers for radiation-protective structural composites. *Nanotechnologies Constr.* **2016**, *8*, 21–37. [CrossRef]
43. McCollom, T.M.; Bach, W. Thermodynamic constraints on hydrogen generation during serpentinization of ultramafic rocks. *Geochim. Et Cosmochim. Acta* **2009**, *73*, 856–875. [CrossRef]
44. Potapov, V.; Gorev, D. Comparative results of concrete compressive strength rising by addition of nanosilica and microsilica. *Mod. High Technol.* **2018**, *9*, 98–102. [CrossRef]
45. Nizina, T.A.; Balykov, A.S.; Korovkin, D.; Volodin, V. Optimization of compositions of cement fiber fine-grained concretes containing carbon nanomodifiers. *Nanoindustry Russ.* **2017**, *78*, 82–91. [CrossRef]
46. Fenter, P.A. X-ray Reflectivity as a Probe of Mineral-Fluid Interfaces: A User Guide. *Rev. Mineral. Geochem.* **2002**, *49*, 149–221. [CrossRef]
47. Lukpanov, R.; Dyussembinov, D.; Altynbekova, A.; Zhantlesova, Z. Research on the effect of microsilica on the properties of the cement-sand mixture. *Technobius* **2022**, *2*, 0027. [CrossRef]
48. Faghihmaleki, H.; Nazari, H. Laboratory study of metakaolin and microsilica effect on the performance of high-strength concrete containing Forta fibers. *ABEN* **2023**, *4*, 11. [CrossRef]